Research paper

Rationally designed divalent caffeic amides inhibit amyloid-β fibrillization, induce fibril dissociation, and ameliorate cytotoxicity

Ling-Hsien Tu [a, 1, 2], Ning-Hsuan Tseng [a, 1], Ya-Ru Tsai [b, 1], Tien-Wei Lin [a], Yi-Wei Lo [a], Jien-Lin Charng [a], Hua-Ting Hsu [a], Yu-Sheng Chen [b], Rong-Jie Chen [a], Ying-Ta Wu [a], Yi-Tsu Chan [b], Chang-Shi Chen [c], Jim-Min Fang [a, b, *], Yun-Ru Chen [a, **]

[a] Genomics Research Center, Academia Sinica, Taipei, 115, Taiwan
[b] Department of Chemistry, National Taiwan University, Taipei, 106, Taiwan
[c] Department of Biochemistry and Molecular Biology, National Cheng Kung University, Tainan, Taiwan

ABSTRACT

One of the pathologic hallmarks in Alzheimer's disease (AD) is extracellular senile plaques composed of amyloid-β (Aβ) fibrils. Blocking Aβ self-assembly or disassembling Aβ aggregates by small molecules would be potential therapeutic strategies to treat AD. In this study, we synthesized a series of rationally designed divalent compounds and examined their effects on Aβ fibrillization. A divalent amide (**2**) derived from two molecules of caffeic acid with a propylenediamine linker of ~5.0 Å in length, which is close to the distance of adjacent β sheets in Aβ fibrils, showed good potency to inhibit Aβ(1–42) fibrillization. Furthermore, compound **2** effectively dissociated the Aβ(1–42) preformed fibrils. The cytotoxicity induced by Aβ(1–42) aggregates in human neuroblastoma was reduced in the presence of **2**, and feeding **2** to Aβ transgenic *C. elegans* rescued the paralysis phenotype. In addition, the binding and stoichiometry of **2** to Aβ(1–40) were demonstrated by using electrospray ionization–traveling wave ion mobility–mass spectrometry, while molecular dynamic simulation was conducted to gain structural insights into the Aβ(1–40)–**2** complex.

© 2018 Elsevier Masson SAS. All rights reserved.

1. Introduction

Aβ peptide composed of 40 or 42 residues is generated from proteolysis of amyloid precursor protein by β- and γ-secretases. Aβ aggregation is highly implicated in Alzheimer's disease (AD)

pathogenesis [1]. Aβ is an intrinsically disordered and highly aggregation-prone peptide. Aβ fibrillization starts with a lag phase in which the protein monomers gradually associate into soluble oligomers, and followed by a rapid elongation phase of fibril formation to reach a steady phase where mature amyloid fibrils are formed. The structure of Aβ fibrils has been revealed at different levels. Aβ(1–42) fibrils consist of three parallel β-sheets (i.e. aa 12–18, 24–33, and 36–40) [2,3], which are different from the Aβ(1–40) fibril comprising two parallel β-sheets (i.e. aa 10–22 and 30–40) [4]. The distance of ~4.7 Å of intermolecular in-register β-sheets derived from the measurement of two adjacent carbonyl groups by solid-state nuclear magnetic resonance (NMR) is consistent with a typical cross-β diffraction pattern revealed by X-ray fiber diffraction [5]. The amyloid positron-emission tomography (PET) tracers are currently used for probing the fibril amount in brain of the patients to monitor the progression of Alzheimer's disease [6]. The process of Aβ aggregation has been suggested to induce synaptic dysfunction and cause neurotoxicity [7]. Even though Aβ(1–40) is more abundant than Aβ(1–42) in AD patient's brain, Aβ(1–42) aggregates more aggressively and exhibits

markedly higher toxicity [8,9]. Since Aβ aggregation is apparently a key target for AD treatment, many researchers aim to develop therapeutic approaches that prevent production of Aβ peptides or inhibit their abnormal aggregation [10−12].

Screening or designing small drug-like molecules targeting Aβ has been considered as one of the promising strategies for therapeutics of AD [13]. The concepts include that small molecules disrupt protein−protein interactions among Aβ monomers, stop conformational change of Aβ from its intermediates to β-sheet fibrillar state, and indirectly inhibit Aβ aggregation by sequestering excess metals [14]. Previous studies have identified small molecules such as Congo red [15], chrysamine G [16], and curcumin [17−22] as potent inhibitors of Aβ. These inhibitors share a similar chemical motif containing two substituted aromatic groups to bind with Aβ. It suggests that an ideal Aβ inhibitor should contain terminal groups interacting with the residues in or adjacent to the segments that are considered crucial for peptide aggregation. Thus, the linker should have an appropriate length to join the two terminal aromatic groups spanning the segments. In another aspect, caffeic acid (CA), a chemical constituent widely distributed in edible plants, is also found to protect neuronal cells from Aβ-induced cytotoxicity [23], presumably because the catechol moiety can provide hydrogen bonding and hydrophobic interaction with Aβ peptide. Inspired by these findings, we thus designed and synthesized a series of divalent compounds based on the scaffold of CA to examine their effects on Aβ fibrillization.

2. Results

2.1. Design and synthesis of divalent compounds

To take advantage of multivalent effect on enhancement of binding affinity [24], the divalent compounds **1**−**11** (Fig. 1) were designed as possible inhibitors against formation of Aβ fibrils. Five dimeric CA amides **2**−**6** are equipped with different lengths of straight-chain linkers. The linkers include propylenediamine (a short linker of ~5.0 Å length) and a series of ethylene glycol diamines (up to ~22.5 Å length). The linkers are chosen for easy linkage to two CA motifs, thus the prepared dimeric compounds would have good solubility in PBS buffer. In comparison, the dimeric CA molecules **7**−**10** have more rigid linkers by incorporation of phenyl and triazole rings. CA is a catechol-containing molecule, whereas curcumin molecule contains monomethylated catechol rings. Compound **1** (R = H), the demethylated derivative of curcumin (**12**, R = Me), is also designed because it shares the structural feature similar to that of divalent caffeic compound. Rosmarinic acid (RA) is a natural compound structurally formed by addition of CA to the double bond of another CA molecule. It would be interesting to synthesize a dimeric RA compound **11** and examine its binding potency with Aβ.

Scheme 1 shows the synthetic pathways to the divalent compounds **1**−**11**. Demethylation of curcumin was readily accomplished by treatment with Lewis acid BBr₃ to give compound **1** [25].

The coupling reaction of diamine linker with two molecules of CA was carried out by the promotion of 1-ethyl-3-(3-dimethylaminopropyl) carbodiimide (EDCI) and 1-hydroxybenzotriazole (HOBt) in *N,N*-dimethyl formamide (DMF) solution. The crude coupling products were subjected to acetylation, followed by deprotection of the acetyl groups, to facilitate isolation of the dimeric CA compounds **2**−**6**. Alternatively, the amines **14**−**16** containing a terminal alkynyl group were reacted with CA to afford amides **17**−**19**, which underwent a Cu(I)-catalyzed (3 + 2) dipolar cycloaddition [26] with bis-azides **20** or **21** to furnish the triazole formation, giving compounds **7**−**10**. The coupling reaction between rosmarinic acid and amine **14** was

realized by the promotion of benzotriazol-1-yl-oxy-tripyrrolidinophosphonium (PyBop) to afford compound **23**, which was subsequently treated with linker **21** to give the dimeric RA compound **11** via click reaction [26].

2.2. Inhibition of Aβ fibrillization

Thioflavin T (ThT) assay was employed to monitor the inhibitory effect of the synthetic dimeric compounds on Aβ aggregation. ThT is a classic amyloid dye that binds to crossed β-sheets of amyloid fibrils and emits fluorescence upon fibril formation [27]. The percentage of fibril formation corresponding to the presence of individual test compound was calculated from the relative intensity of fluorescence at 485 nm, compared with 100% fibril formation in phosphate buffer (pH 7.4). Our initial screening of compounds **1**−**11** indicated that the dimeric compound **2** was an effective inhibitor at a concentration of 10 μM, rendering about 50% reduction of Aβ(1−40) fibrillization (Table 1).

The inhibitory activities of divalent caffeic amides **3**−**10** varied depending on the types and lengths of linkers. The one-arm compounds, such as caffeic acid (**13**) and its amide derivatives **17**−**19**, were less effective inhibitors. Rosmarinic acid (**22**) showed a relatively low inhibitory activity [20], and its amide derivative **23** was inactive at 10 μM. Nonetheless, the Aβ inhibitory activity was enhanced in dimeric RA compound (**11**). Demethylated curcumin (**1**) in PBS solution likely exists as the enol tautomer to have an absorption band at $\lambda_{max} = 437$ nm, which would interfere with the ThT assay using 442 nm light for excitation. Thus, the real inhibitory activity of **1** against Aβ fibril formation could not be determined by this ThT assay.

Since Aβ(1−42) is a more aggressive and toxic Aβ isoform than Aβ(1−40), we investigated the efficiency of curcumin (**12**), CA (**13**) and dimeric CA (diCA, **2**) on preventing Aβ(1−42) fibrillization. The solution of Aβ(1−42) at 50 μM with 5 μM ThT was co-incubated individually with 100, 25, 12.5, 3.1, 0.8, 0.1 and 0.01 μM of test compound at 37 °C. The ThT intensity was monitored for a period over 80 h. We found that all three compounds could inhibit the fibrillization of Aβ(1−42) in a dose-dependent manner (Fig. 2a−2c). The normalized final ThT intensity (at 80 h incubation) was plotted against compound concentration and the data were fitted to obtain half maximal inhibitory concentration (IC₅₀) for compounds **2** (IC₅₀ = 4.9 ± 0.08 μM), **12** (IC₅₀ = 3.4 ± 0.07 μM) and **13** (IC₅₀ = 15.6 ± 0.13 μM) (Fig. 2d).

Next, morphology of the end-point products after 80 h incubation was examined by transmission electron microscopy (TEM). In the absence of test compound, the Aβ(1−42) sample formed clustered and dense fibrils (Fig. 3a). In contrast, when Aβ(1−42) was co-incubated with 25 μM of test compound, no fibril was found and only some amorphous aggregates appeared (Fig. 3b−3d). Also, when Aβ(1−42) was co-incubated with 12.5 μM of test compound, only a few fibrils and short filaments were observed (Fig. 3e−g).

To find the influence of linker length in inhibition of Aβ(1−42) fibrillization, we compared the binding affinity of dimeric CA amides **2**−**6**. Aβ(1−42) was first prepared at 50 μM in the presence of ThT, and then co-incubated individually with test compound at 0.8, 3.1, 12.5, 25 and 100 μM at 37 °C. The ThT intensity was normalized with that of Aβ(1−42) alone (Fig. S1a in Supporting Information). Although all the CA dimers can affect Aβ(1−42) fibrillization with increasing concentration, compound **2** with ~5.0 Å linker greatly reduced the final ThT intensity, suggesting that compound **2** has good potential to inhibit Aβ(1−42) fibril formation. When 50 μM Aβ(1−42) was incubated with 3.1 μM of **2**, the final ThT intensity of Aβ(1−42) with the compound was reduced to ~60% compared with that of Aβ fibrils only. With increase of the inhibitor **2** to 25 and 100 μM concentrations, the final ThT intensity
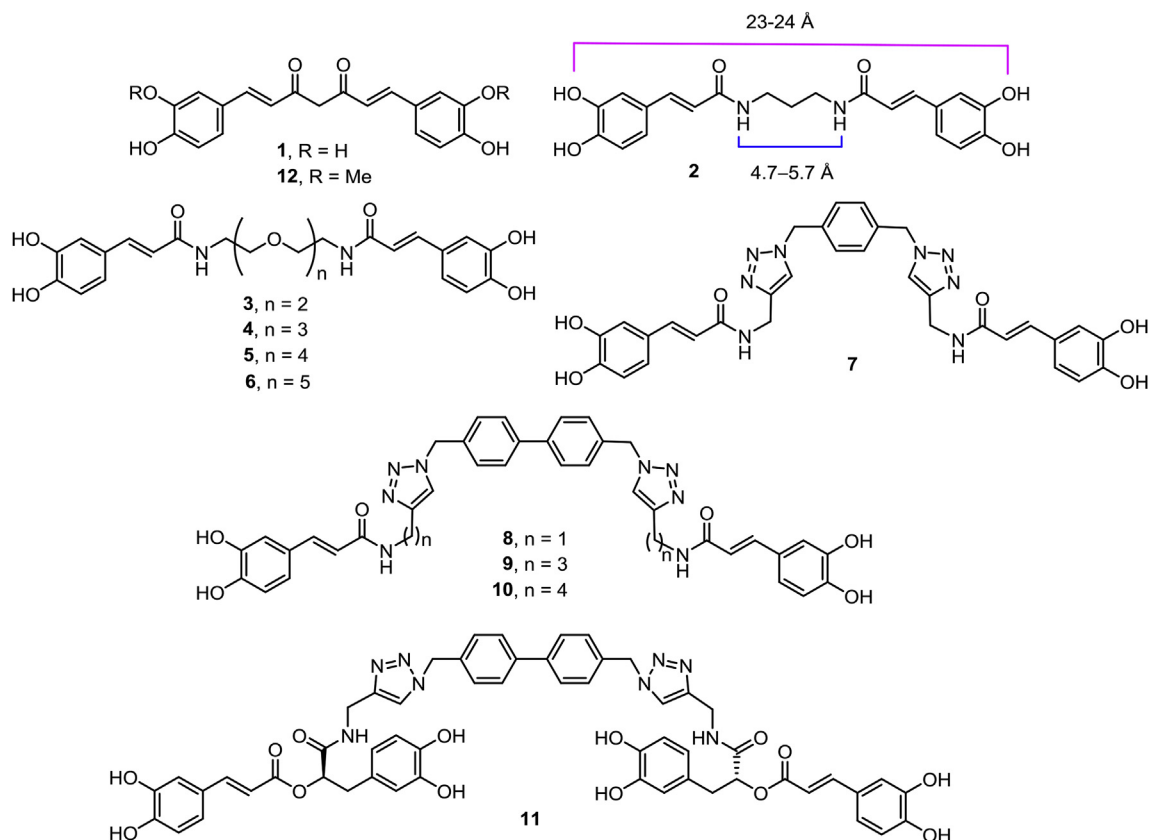
Fig. 1. Structures of divalent compounds derived from the scaffold of caffeic acid. The length of diamine linker and the distance between two catechol groups in compound **2** were estimated by ChemDraw 15.0 software (PerkinElmer).

significantly reduced to ~8% and ~1%, respectively. We also confirmed the ThT results by taking TEM images. All the images were recorded for Aβ with and without 12.5 μM CA dimers. The result showed that all Aβ(1—42) peptides formed long and extensive fibrils in the absence (Supplementary Fig. S1b) and presence of most CA dimers (Supplementary Fig. S1d—g) except for compound **2** (Supplementary Fig. S1c). Incubation of Aβ(1—42) with compound **2** only led to formation of some short filaments.

2.3. Compound **2** disassembles Aβ fibrils

In addition, we examined the ability of diCA (**2**) in disassembling preformed Aβ fibrils. Aβ(1—42) fibrils were first prepared at 25 μM. Then, diCA at different concentrations, ranging from 0 to 100 μM, was added into the preformed fibrils with 5 μM ThT, and the change of ThT fluorescence was monitored with buffer background subtracted (Fig. 4a). We found Aβ(1—42) fibrils alone have some decrease in ThT intensity which may be due to gradual sedimentation of fibrils and/or clustering of Aβ(1—42) fibrils after a period of time. Interestingly, we found that diCA is able to reduce mature fibrils in a dose-dependent manner with IC_{50} of 4.2 ± 0.03 μM (Fig. 4b). Since fluorescence signal may be affected by environment and binding mode, we further confirmed the Aβ assembly by loading the samples in the absence and presence of different concentrations of **2** (25, 50 and 100 μM) at time 0 and after 14 days of incubation to native Tris-tricine gel and subjected to western blot (Fig. 4c) and TEM (Fig. 4d and e) examination. The western blot results showed that there is a slight reduction of aggregates in the presence of different concentrations of **2** at time 0. After 14 days of incubation with **2** there are much less or even no aggregates on the

gel. We also confirmed that little filaments were observed when Aβ(1—42) fibrils were incubated with 100 μM of **2** after 14 days in TEM images (Fig. 4e) whereas Aβ(1—42) fibrils with 100 μM of **2** at time 0 still remained at least in some degree as dense fibrils (Fig. 4d). The result showed that the CA dimer **2** reduced the preformed Aβ fibrils as evidence by reduced ThT intensity, reduced aggregates on the top of western blots, and reduced fibrils in TEM images.

2.4. Compound **2** binds to Aβ monomer and oligomers

To understand the molecular interaction of CA dimer **2** with Aβ, we utilized electrospray ionization—traveling wave ion mobility—mass spectrometry (ESI-TWIM-MS) to detect the possible complexes formed by Aβ with compound **2**. ESI-TWIM-MS has been widely utilized in differentiating isomeric structures with similar sizes [30,31]. By applying voltage pulses in the ion-mobility cell, the ions are propelled to drift against a stream of buffer gas [32,33]. The time that ions need to drift through the ion-mobility cell is dependent on their *m/z* ratios and molecular shape. At the same *m/z* ratio, the more compact ion reveals a shorter drift time so that isomer differentiation can be realized. This technique has been frequently utilized in characterizing the ion species in a complex mixture. Thus, one can use ESI-TWIM-MS to examine the binding capacity of ligands to target protein. Recently, several binding modes classified from a series of small molecules inhibitors against Aβ(1—40) and islet amyloid polypeptide indicated that the potent inhibitors usually can bind protein in a stoichiometric manner [34]. Due to fast aggregation of Aβ(1—42) that would complicate the ESI-TWIM-MS experiment, Aβ(1—40) is commonly used to investigate
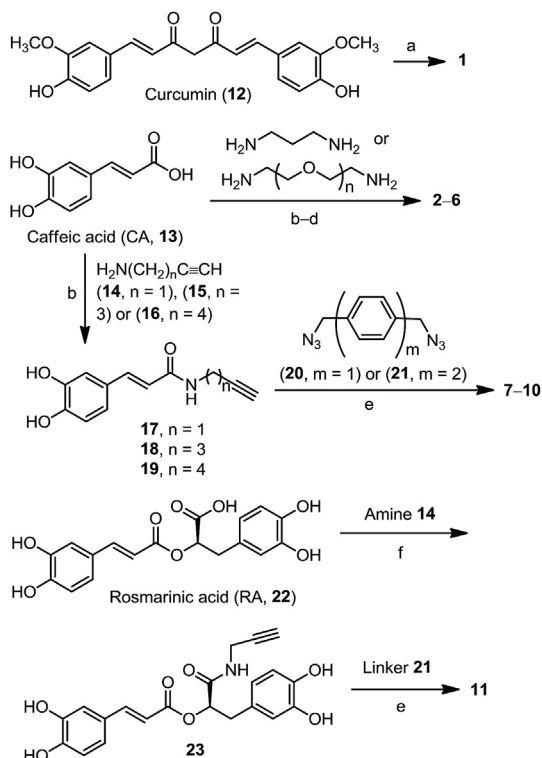
Scheme 1. Synthesis of divalent compounds **1**—**11**.[aa] Reagents and reaction conditions: (a) BBr$_3$, CH$_2$Cl$_2$, −78 °C (15 min), rt (12 h); 63%. (b) EDCI, HOBt, Et$_3$N, DMF, rt, 18 h; **17**, 93%; **18**, 71%; **19**, 51%. (c) Ac$_2$O, py, rt, 12 h (d) K$_2$CO$_3$, MeOH, rt, 0.5 h; **2**, 27%; **3**, 58%; **4**, 58%; **5**, 36%; **6**, 34%. (e) CuSO$_4$, sodium ascorbate, THF/H$_2$O (1:1), 40 °C, 12 h; **7**, 67%; **8**, 26%; **9**, 59%; **10**, 20%; **11**, 52%. (f) PyBop, Et$_3$N, DMF, rt, 18 h; 62%.

Table 1
Effect of test compounds against fibril formation of Aβ(1—40).[a]

compound	fibril formation (%)[a]	compound	fibril formation (%)[a]
1	11.5 ± 0.4[b]	**10**	61.8 ± 2.5
2	52.9 ± 2.5	**11**	65.1 ± 10.6
3	64.7 ± 5.6	**13**	91.2 ± 9.1
4	79.4 ± 2.5	**17**	79.4 ± 6.1
5	61.8 ± 2.0	**18**	135.3 ± 7.6
6	67.6 ± 4.1	**19**	67.6 ± 6.1
7	76.5 ± 7.8	**22**	79.1 ± 7.6
8	88.2 ± 1.5	**23**	107.0 ± 1.0
9	111.8 ± 2.5		

[a] Aβ(1—40) of 25 μM in PBS (pH 7.4) was incubated with test compound (10 μM), and the fibril formation was monitored by ThT assay. The percentage of fibril formation was calculated from the relative intensity of fluorescence emission at 485 nm by excitation at 442 nm wavelength. Control is PBS, corresponding to 100% fibril formation in the absence of test compound. The experiments were performed in duplicate.

[b] The percentage of fibril formation was likely underestimated because compound **1** (the demethylated derivative of curcumin) in PBS had UV absorption band at λ_{max} = 437 nm (ε = 2600 M^{-1}cm^{-1}), which would interfere with ThT assay using excitation wavelength of 442 nm.

its molecular interactions with ligands. In our study, Aβ(1—40) alone at 35 μM or with 200 μM of compound **2** in a 1:5.7 M ratio (Aβ/**2**) were prepared and injected for recording the ESI-TWIM-MS spectra. The experiments revealed that Aβ(1—40) yielded dominantly the 3 + and 4 + monomeric ions as well as the 4 + and 5 + dimeric ions, appearing at m/z 1444, 1083, 2166, and 1733, respectively (Table 2). The result is consistent with the previous literature [34]. When diCA (**2**) was present in the Aβ(1—40) solution, one to four diCA molecules were found to bind with 3 + ion of

Aβ(1—40) monomer and one to three diCA molecules were detected to be with 4 + and 5 + ions of Aβ(1—40) dimer (Fig. 5 and Table 2). The 3 + ions of Aβ−**2** complexes at 1:1, 1:2 and 1:3 stoichiometry which occurred at m/z = 1576, 1709, and 1842, respectively, were indicated by orange stars in Fig. 5a and b. In addition, Aβ dimer and their diCA complexes of 2:1 and 2:2 stoichiometry in both 4 + and 5 + states were also resolved (Table 2), indicating that the binding mode of diCA to Aβ(1—40) monomer or dimer is specific. The collision cross-section (CCS) value of each complex was calculated and listed in Table 2.

In an attempt to elucidate the structural basis for binding of Aβ with diCA (**2**) by nuclear magnetic resonance (NMR) spectroscopy [28,29], we acquired the ^{1}H—^{15}N heteronuclear single quantum coherence (HSQC) spectrum (Supplementary Fig. S2). Despite compound **2** is a good inhibitor against Aβ fibrillization, we did not observe apparent change of chemical shifts from cross peaks of ^{15}N-labeled Aβ(1—42) at 25 μM when it was incubated with **2** at 500 μM. The reason for insignificant change in the HSQC spectrum is unclear; however, similar phenomena have been shown in other inhibition studies [28,29]. One possible explanation is that the interaction between compound **2** and Aβ(1—42) is transient and may be at a relatively low concentration that cannot effectively induce NMR chemical shifts. No further NMR experiment was attempted in this study.

Alternatively, we employed computational methods to obtain the structural insights into the complexation of Aβ monomer with ligand **2**. Since Aβ monomer is natively disordered, the only available PDB file for Aβ(1—40) was determined by NMR (PDB code 2LFM) and used for molecular docking experiment. According to our docking results, 9 dominant conformations of Aβ−**2** complex were revealed. The small molecule **2** seems to preferentially interact with Aβ near the α-helical region and disrupt the partially folded helix structure. We also conducted molecular dynamic (MD) simulations based on 11 docked structures of Aβ−**2** complex to identify the possible conformers observed in our ESI-TWIM-MS experiments. From MD trajectory, a hundred structures were sampled from each starting complex. Each conformation was converted to the corresponding CCS by the trajectory method (TM) in MOBCAL [35]. Their optimized potential force field energy and individual orientationally averaged CCS values were also calculated (Fig. S3). Comparing the CCS values in ESI-TWIM-MS experiment and MD simulation, most of the calculated CCS values for the complex derived from MD simulation are larger than our experimental data (e.g., 634 Å^2 for a 3 + state of Aβ−**2** complex in Table 2). However, we still found several similar conformers whose CCS values matched well to our experimental data. Hence, two groups of representative Aβ−**2** complex are depicted in Fig. 5c and d.

2.5. Compound **2** ameliorates Aβ(1—42) induced cytotoxicity

To examine possible rescue effect of diCA (**2**), the end-point products of Aβ(1—42) in ThT assay after incubation with and without test compound at different concentrations were treated to human neuroblastoma SH-SY5Y cells and subjected to cytotoxicity assay. After 48 h incubation, cytotoxicity was assessed by lactate dehydrogenase (LDH) assay (Fig. 6a). The LDH assay showed that Aβ(1—42) fibrils induced ~49% cytotoxicity and this deleterious effect was gradually attenuated after co-incubating with curcumin (**12**), CA (**13**) or diCA (**2**) in a dose dependent manner. Among all concentration tested, diCA is the most potent compound in comparison to the others. At 0.01 μM, diCA was able to reduce cytotoxicity from 49% to 30% (rescue ~19%), whereas CA was only able to rescue ~5% and curcumin has no effect at this concentration. At 25 μM, diCA was able to reduce cytotoxicity from 49% to 15% (rescue ~34%), whereas CA and curcumin were able to reduce cytotoxicity
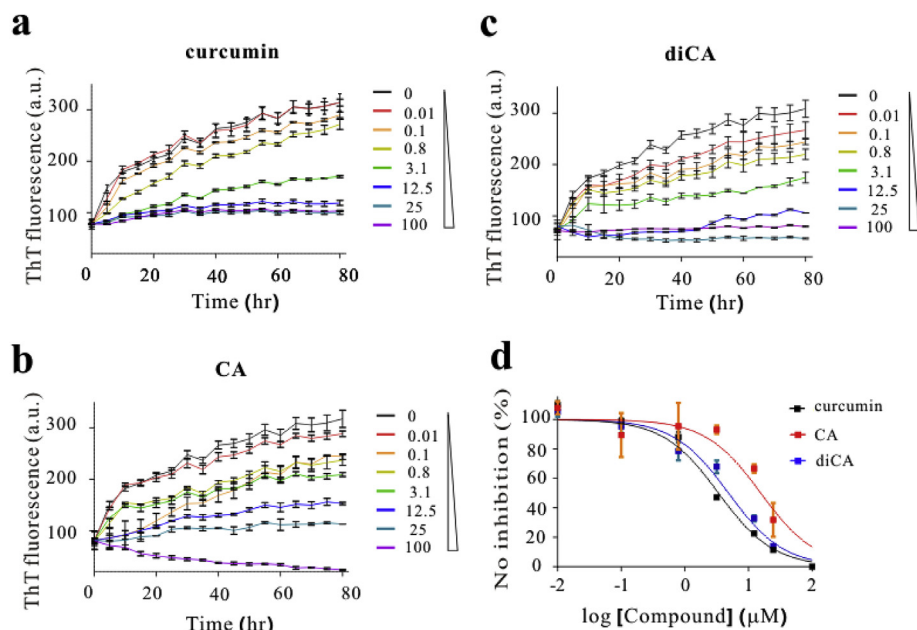
Fig. 2. The inhibitory effect of curcumin (**12**), caffeic acid (**13**), and divalent caffeic amide (diCA, **2**) on Aβ(1−42) fibrillization. Fibrillization of Aβ(1−42) in the presence of (a) **12**, (b) **13**, and (c) **2** were monitored by ThT assay. The fluorescence intensity was recorded (λ_{ex} = 442 nm, λ_{em} = 485 nm). Experiments in triplicate were performed in 20 mM phosphate buffer (pH 7.4) at 37 °C containing 50 μM Aβ(1−42) in the absence or presence of 0.01, 0.1, 0.8, 3.1, 12.5, 25, and 100 μM compounds. Mean value and standard error of mean (SEM) were shown for each time point. (d) The percentage of inhibition calculated from the final normalized ThT signals was plotted against compound concentration. The data were fit to an equation Y = 100/(1 + 10^(X-LogIC$_{50}$)) to calculate IC$_{50}$ values. SEM was shown; however, some are too little to be seen.
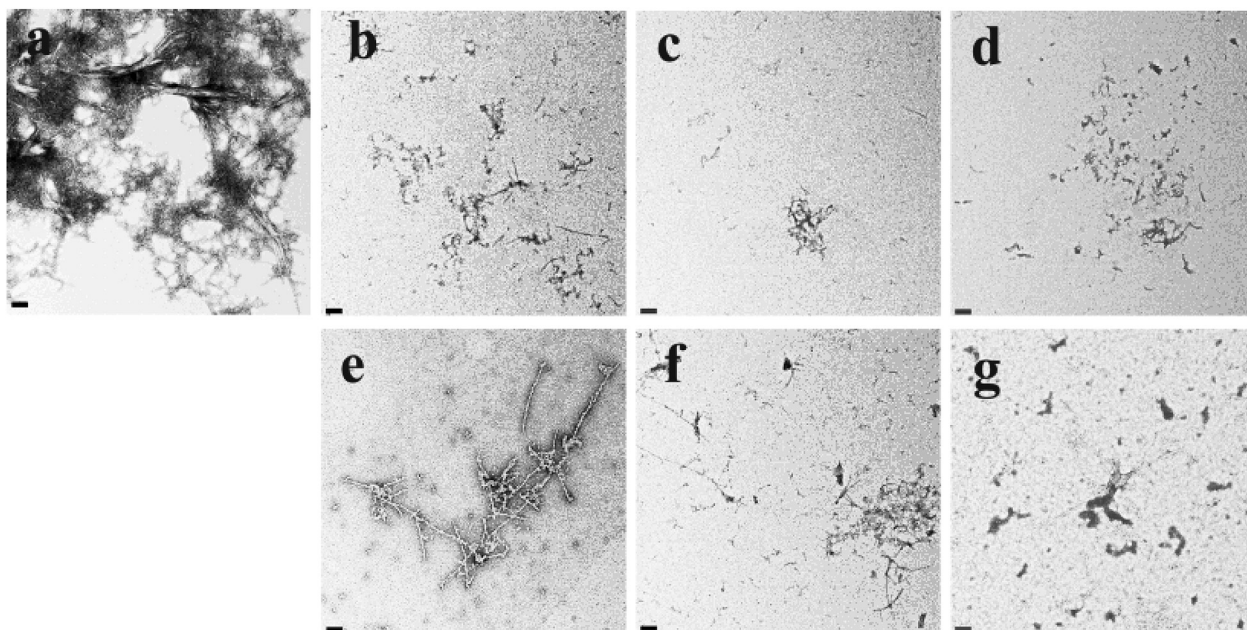

Fig. 3. TEM images of 50 μM Aβ(1−42) after incubation in the absence and presence of test compounds. Aβ(1−42) in the absence of test compound (a) and in the presence of 25 μM curcumin (b), CA (c), and diCA (d). Aβ(1−42) in the presence of 12.5 μM curcumin (e), CA (f), and diCA (g). The scale bar represents 100 nm.

from 49% to ~27% (rescue ~22%). Although all three compounds were able to rescue Aβ(1−42) induced toxicity, diCA provided the most beneficial effect even at low concentration.

To understand whether diCA could rescue the cytotoxicity induced by preformed Aβ fibrils, we first prepared Aβ(1−42) fibrils in the absence and presence of diCA at different concentrations (0, 25, 50 and 100 μM). The samples were then treated to SH-SY5Y cells

and subjected to LDH assay (Fig. 6b). The result showed that Aβ(1−42) fibrils alone caused cytotoxicity about 17%, while fibrils in the presence of 50 and 100 μM diCA could significantly reduce fibril-induced cytotoxicity to 12% and 9%. Though Aβ fibrils in the presence of 25 μM diCA did not reduce the cytotoxicity, our study still demonstrated that diCA at appropriate concentration was able to rescue cytotoxicity induced by preformed Aβ(1−42) fibrils.
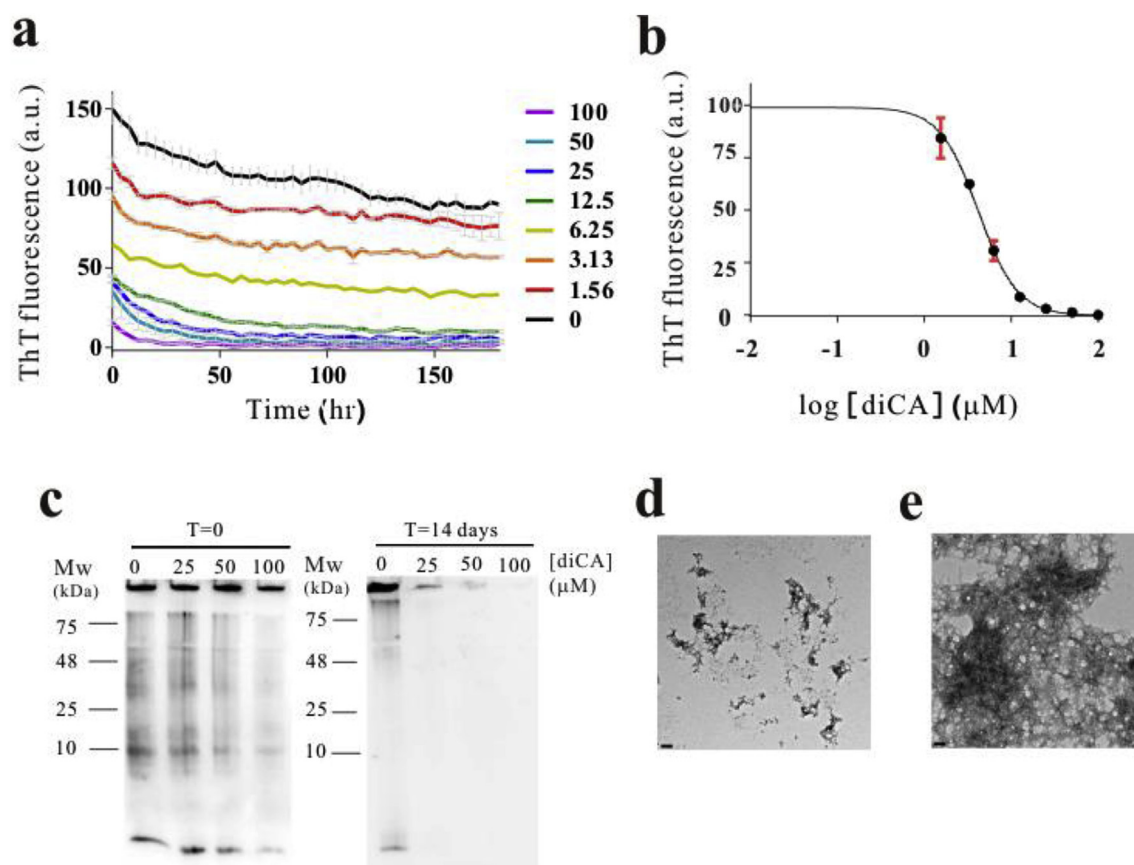
Fig. 4. Compound **2** (diCA) disassembles preformed Aβ(1–42) fibrils. (a) Preformed Aβ(1–42) fibrils were incubated with 0–100 μM diCA solution containing 1% DMSO and 5 μM ThT. The assay was performed in triplicate. (b) The final ThT fluorescence intensity (buffer background subtracted) in the presence of diCA was normalized to Aβ(1–42) fibrils alone and plotted with the log value of compound concentration. The data in three sets were fit to an equation $Y = 100/(1 + 10^\wedge(\text{X-LogIC}_{50}))$ to calculate IC$_{50}$ value. (c) Aβ(1–42) fibrils with 0, 25, 50 and 100 μM diCA were incubated for 0 and 14 days, and the aggregates were visualized by gel electrophoresis with western blotting probed by anti-Aβ antibody 4G8 and 6E10. (d) TEM image of Aβ(1–42) fibrils with 100 μM diCA without incubation. (e) TEM image of Aβ(1–42) fibrils with 100 μM diCA after 14 days incubation. The scale bar represents 100 nm.

Table 2
Experimental mass to charge ratio, drift time and collision cross-section (CCS) of Aβ(1–40) and its complexation species with diCA (**2**).

species[a]	charge state	m/z	drift time (ms)	CCS (Å^2)
M	4+	1083.2816	9.81	695.2
M	3+	1444.0408	12.24	602.9
M+L	3+	1576.7568	13.23	633.8
M+2L	3+	1709.8217	14.33	668.4
M+3L	3+	1842.5073	15.44	699.3
M+4L	3+	1975.2498	16.43	727.3
2M	5+	1733.0510	11.69	973.3
2M+L	5+	1812.6821	12.02	991.0
2M+2L	5+	1892.5221	12.35	1008.4
2M+3L	5+	1971.7124	13.01	1042.9
2M	4+	2165.8137	15.99	952.4
2M+L	4+	2265.1050	16.65	977.0
2M+2L	4+	2365.1323	17.31	1001.2

[a] M represents Aβ(1–40); 2M represents dimer of Aβ(1–40); L represents diCA (**2**).

2.6. Compound **2** significantly rescues Aβ(1–42) induced cytotoxicity in transgenic C. elegans and extends their lifespan

We further examined the *in vivo* efficacy of test compounds by feeding them to transgenic *Caenorhabditis elegans* that expresses Aβ(1–42) in muscle under temperature regulation. When temperature shifts above 25 °C, Aβ peptides start to express and accumulate in the muscle system, leading to paralysis and death of *C. elegans*. Thus, the percentage of paralysis and survival time of *C. elegans* can be taken as indications of the efficacy of test compound in treatment of AD *C. elegans*.

At first, the worms were cultured and treated with individual compound at 16 °C. After 20 h, we increased temperature to upregulate transgenic expression, which caused paralysis and death of *C. elegans* within 12 h. Over 100 worms were examined with or without paralysis in each condition, and the percentages of worms without paralysis were plotted against time. The result showed that pretreatment with test compounds, especially diCA (**2**), significantly delayed the onset of Aβ-induced paralysis (Fig. 7). At 26 h, the survival rate of worms treated with diCA (67.9%) was 2.5 fold increase compared with those treated in buffer (27.6%) (Fig. 7a). The median survival time, which is a measure of 50% survival of worms, was also analyzed, showing 25.7, 26.3 and 27.3 h in treatment with curcumin, CA and diCA, respectively, compared with 24.2 h in buffer (control). The worms fed with diCA were able to increase the median survival time for 3.1 h more than the buffer control. The result strongly supported that diCA (**2**) is a potent compound to suppress Aβ toxicity (Fig. 7b), in agreement with the *in vitro* cellular experiment. Overall, we confirm that diCA is significantly more potent than curcumin and CA in reducing the toxicity of Aβ *in vitro* and *in vivo*.
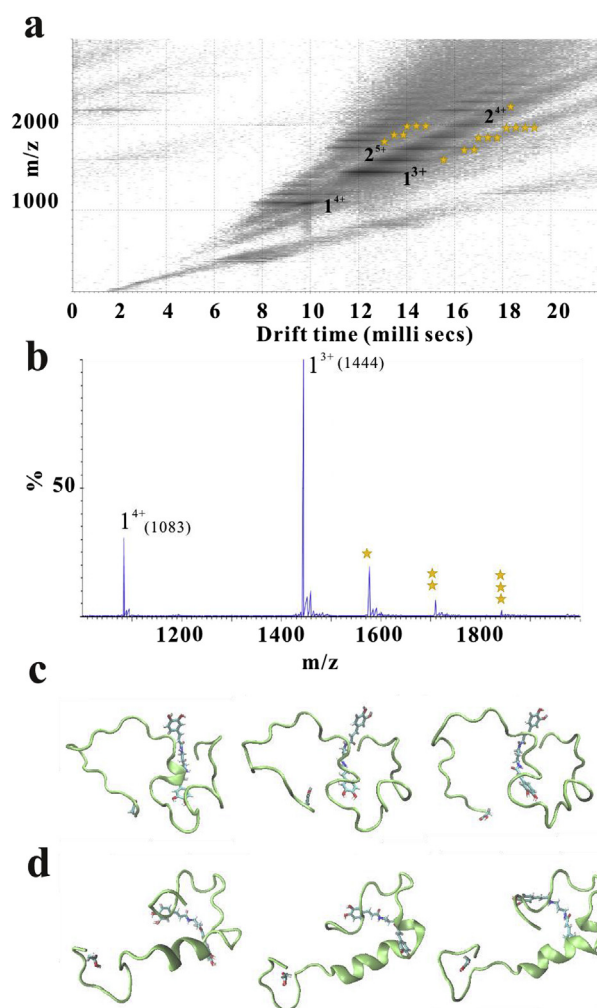
Fig. 5. ESI-TWIM-MS and MD simulation of the complexation species of Aβ(1–40) with diCA (**2**). (a) ESI-TWIM-MS plot of 35 μM Aβ(1–40) with 200 μM diCA in 50 mM ammonium acetate (pH 6.8). DiCA binds to the 3 + ion of Aβ monomer and to the 4 + and 5 + ions of Aβ dimer. Aβ and diCA complexes are indicated by orange stars, and the number of orange stars represents the number of diCA bound to Aβ. (b) The positive-mode ESI mass spectrum of Aβ(1–40) with diCA. Monomeric Aβ and its diCA complexes are shown. (c) & (d) represent the two groups of diCA and Aβ complex structures from MD simulation. The side chain of first amino acid residue in Aβ(1–40) is shown. The calculated CCSs match our experimental data. (For interpretation of the references to colour in this figure legend, the reader is referred to the Web version of this article.)

3. Discussion

Caffeic acid (CA), a catechol-containing small molecule with a single ring has shown its potential in prevention of Aβ aggregation. Other catechol-containing compounds, such as gallic acid, dopamoin, and pyrogallol, seem to have similar effects [36]. To develop better inhibitors for AD therapy, we synthesized a series of divalent compounds based on the structure of CA to attain possible multivalent effect. The chemical scaffold of our designed small molecules contains two catechol end groups that are connected with various types and lengths of linkers. With a concern on that the catechol moiety may cause pan assay interference (PAIN), most of our studies also included curcumin, which is devoid of catechol moiety, as positive control.

Among the divalent compounds synthesized in this study, we found diCA (**2**) with a propylenediamine linker of ~5.0 Å length efficiently inhibited Aβ fibrillization *in vitro*. The inhibitory effect of divalent caffeic amide **2** (IC$_{50}$ = 4.9 μM) is indeed better than monovalent CA (IC$_{50}$ = 15.6 μM) against Aβ(1–42) fibrillization.

To date, various Aβ regions have been proposed for Aβ oligomerization and aggregation. For example, residue 13–16 (HHQK) contributes to Aβ oligomerization and neurotoxicity [37,38], and binding to glycosaminoglycans [39,40]. The hydrophobic core, residue 17–21 (KLVFF) and 32–42 (IGLMVGGVVIA) are considered as crucial motifs that force Aβ to assembly [41–43]. In addition, the flexible hinge or turn region including residue 22–31 is also important in bringing two hydrophobic segments close to each other for formation of the β-sheet structure. Interference with these regions could disrupt Aβ aggregation [19].

Among the dimeric caffeic amides **2**–**10**, their Aβ inhibitory activities varied depending on the types and lengths of linkers. Our ESI-TWIM-MS data demonstrated that diCA (**2**) could bind to Aβ(1–40) and form relative stable complexes since a binomial distribution of the bound protein peaks were observed (Fig. 5b) [34]. The MD simulation revealed that diCA preferentially binds to the central hydrophobic region, a helix from H13 to D23 suggested from a NMR study [44]. Our study indicated that diCA might bind to the helical region of Aβ and disrupted the helical structure, which was visualized in one of our models (Fig. 5). The diCA molecule might also reside in the place near the flexible hinge or turn region. It is known the spacing between two adjacent β-stands in Aβ fibrils is 4.7 Å [2,45,46]. According to our ESI-TWIM-MS experiment, Aβ dimer could form complex with diCA (**2**), which is equipped with a linker of ~5.0 Å length close to the distance between two adjacent β-stands of Aβ fibrils, we speculated that the two catechol moieties in a diCA molecule might concomitantly bind to the hydrophobic regions of Aβ dimers (or oligomers) to inhibit fibril formation. In summary, our study showed that diCA (**2**) is a potent inhibitor against Aβ fibrillization by interacting at different Aβ regions. Finally, by using cell-based assay and AD *C. elegans* model, we have demonstrated that diCA is a superior agent to rescue Aβ toxicity.

In comparison with curcumin that quickly precipitates in PBS buffer at higher concentration, the solubility of our designed molecules is greatly enhanced by incorporating additional hydroxyl groups into the aromatic rings and using the relatively hydrophilic diamine linkers. For example, the diCA sample can be prepared at a concentration up to 0.5 mM in aqueous solution; however, curcumin is not able to maintain in the same level without precipitation. The predicted lipophilicity (clog P) and other physicochemical properties are listed in Table S1. According to Lipinski's rule of five [47], diCA appears to be a drug-like molecule having appropriate physicochemical properties. There is another concern on using ThT assay to evaluate the inhibitory effect of curcumin and its demethylated analog **1** against Aβ fibrillization. In fact, curcumin has been shown to interfere with ThT assay [48], because the absorption band of curcumin is around 425 nm (Supplementary Fig. S4) that partially overlaps with the excitation wavelength of ThT (at 442 nm). Hence, the inhibitory effect of curcumin and analog **1** by ThT assay could be overestimated. In contrast, CA and its dimeric derivatives having the absorptions below 400 nm would not interfere with the ThT assay.

4. Conclusion

In this study, we designed and chemically synthesized a series of divalent compounds based on the structure of CA with various types and lengths of linkers. We found that diCA (**2**) with a linker of ~5.0 Å in length showed the most potent inhibitory effect against Aβ aggregation in comparison to other derivatives with longer or more rigid linkers. Interestingly, diCA can also disassemble preformed Aβ fibrils. We have showed that diCA can bind Aβ in a stoichiometric manner by ESI-TWIM-MS, and obtained insights
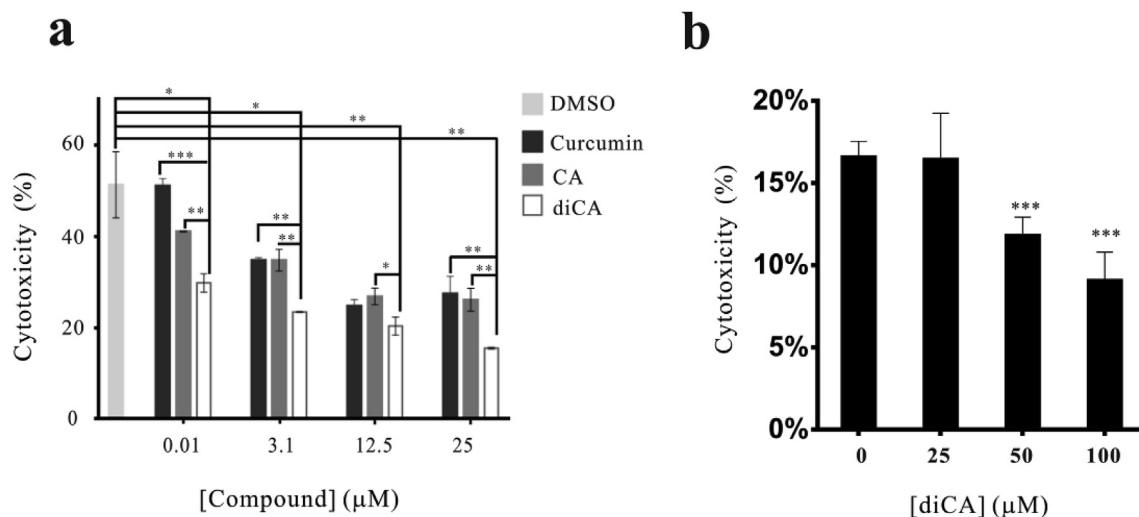
Fig. 6. Rescue effect of test compounds against Aβ(1–42) induced toxicity. (a) Cytotoxicity of Aβ(1–42) in the absence and presence of curcumin (**12**), CA (**13**), and diCA (**2**). The end products of ThT assay were subjected to SH-SY5Y cells and the cytotoxicity was determined by LDH assay. The experiments were performed in triplicate. The data were normalized to the positive control, i.e. cells treated with Triton X-100. The statistical significance was indicated by two-way ANOVA (***, $p < 0.0001$; **, $p < 0.005$; *, $p < 0.05$). (b) Cytotoxicity of preformed Aβ(1–42) fibrils in the presence of diCA. The samples in the absence and presence of diCA at different concentrations were treated to neuroblastoma SH-SY5Y cells. Cytotoxicity was measured by LDH assay. Cells treated with Triton X-100 were used as the positive control for 100% cytotoxicity. The experiments were performed in triplicate. The statistical significance was indicated by one-way ANOVA (***, $p < 0.0001$).
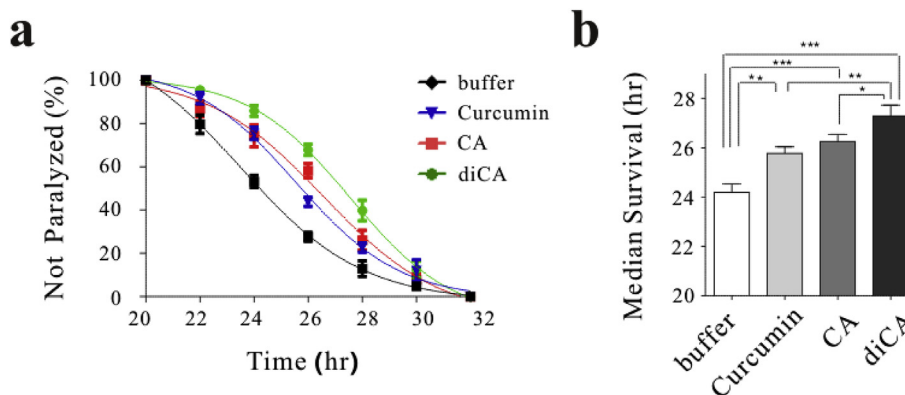

Fig. 7. AD-relevant *C. elegans* model suggests that diCA offers protection from Aβ-induced paralysis. (a) The effect of curcumin (**12**), CA (**13**) and diCA (**2**) on the paralysis phenotype observed in the transgenic *C. elegans* strain CL4176. The number of tested worms is about 100–130. (b) The median survival time was analyzed: buffer (nematode growth media), 24.2 ± 0.4 h; curcumin, 25.7 ± 0.3 h; CA, 26.3 ± 0.3 h; diCA, 27.3 ± 0.4 h. The statistical significance was indicated by one-way ANOVA (***, $p < 0.0001$; **, $p < 0.005$; *, $p < 0.05$).

into the binding modes of Aβ with diCA by MD simulations. Furthermore, diCA is capable of rescuing Aβ-induced toxicity *in vitro* and *in vivo*. Collectively, diCA is a dimeric caffeic amide that is an effective inhibitor against Aβ aggregation and has beneficial effect against Aβ-induced toxicity. As diCA has the physicochemical properties fitting Lipinski's rule of five for druglikeness, it will be worthwhile to investigate whether diCA can be developed into an orally available drug for AD treatment.

5. Experimental section

5.1. General

All reagents were reagent grade and were used without further purification unless otherwise specified. All solvents were anhydrous grade unless indicated otherwise. Dichloromethane (CH_2Cl_2) was distilled from CaH_2. HFIP and ThT were purchased from Sigma-Aldrich (St. Louis, MO, USA). NaCl were from Amresco (Solon, OH,

USA). All aqueous solutions were prepared in double-distilled Milli-Q water.

All air or moisture sensitive experiments were performed under argon or nitrogen atmosphere. Reactions were monitored by thin-layer chromatography (TLC) on 0.25 mm silica gel 60 F_{254} plates. Compounds were visualized by UV, or using *p*-anisaldehyde, ninhydrin, and phosphomolybdic acid (PMA) as visualizing agents. Silica gel 60 (0.040–0.063 mm particle sizes) and Lichroprep RP-18 (0.040–0.063 mm particle sizes) were used for flash chromatography. Normal-phase preparative TLC on 1 mm or 2 mm silica gel 60 F_{254} plates and reversed-phase preparative TLC on 1 mm silica gel 60 RP-18 F_{254} plates were used for compound purification.

Melting points were recorded on a Yanaco micro apparatus. Optical rotations were measured on digital polarimeter of Japan JASCO Co. DIP-1000. $[\alpha]_D$ values are given in units of 10^{-1}deg cm^2 g^{-1}. Infrared (IR) spectra were recorded on Nicolet Magna 550-II. Absorbance spectra were measured on PerkinElmer Lamda 35 UV–Vis spectrometer. Nuclear magnetic resonance (NMR) spectra

were obtained on Varian Unity Plus-400 (400 MHz) and chemical shifts (δ) were recorded in parts per million (ppm) relative to internal standards: $CHCl_3$ ($\delta_H = 7.24$), $CDCl_3$ ($\delta_C = 77.0$ for the central line of triplet), CH_3OD ($\delta_H = 3.31$), CD_3OD ($\delta_C = 49.15$), $(CD_2H)_2SO$ ($\delta_H = 2.50$), $(CD_3)_2SO$ ($\delta_C = 39.51$), and DHO ($\delta_H = 4.80$). The splitting patterns are reported as s (singlet), d (doublet), t (triplet), q (quartet), m (multiplet) and br (broad). Coupling constants (J) are given in Hz. The ESI−MS experiments were conducted on a Bruker Daltonics BioTOF III high-resolution mass spectrometer. The MALDI-TOF-MS experiments were conducted on UltraFlex II high-resolution mass spectrometer. High-performance liquid chromatography (HPLC) was performed on Agilent 1100 Series instrument equipped with a degasser, Quat pump, and UV detector. The ThT fluorescence assay was detected by SpectraMax M5 Multi-Mode Microplate Readers.

Aβ(1−40) and Aβ(1−42) peptides were synthesized by Fmoc solid-phase peptide synthesis in the Genomics Research Center (Academia Sinica, Taiwan). The peptides were purified by reversed-phase HPLC. The molecular mass was identified by MALDI-TOF-MS.

5.2. Synthetic procedures and compound characterization

Compounds **1** and **2** were prepared according to the previously reported procedure with slight modification [25,49]. The purity of compounds was determined by HPLC on a HC-C18 column (Agilent, 4.6×250 mm, 5 μm particle size) at a flow rate of 1 mL/min with gradient elution of 50% aqueous MeOH.

5.2.1. Representative procedure A for coupling reaction of caffeic acid with diamine linker

A mixture of 3,4-dihydroxycinnamic acid (497 mg, 2.76 mmol), 1-ethyl-3-(3-dimethylaminopropyl) carbodiimide (EDCI) (794 mg, 4.14 mmol), 1-hydroxybenzotriazole (HOBt) (559 mg, 4.14 mmol), Et$_3$N (0.58 mL, 4.14 mmol) in anhydrous DMF (10 mL) was stirred under an atmosphere of argon for 10 min at 26 °C. Propane-1,3-diamine (102 mg, 1.38 mmol) was added, and the mixture was stirred for 18 h at 26 °C. The mixture was concentrated under reduced pressure to give a crude coupling product of the title compound (**2**). To facilitate isolation, the coupling product was treated with Ac$_2$O (10 mL) in pyridine (10 mL) at 26 °C for 12 h. The mixture was concentrated, and extracted with EtOAc and water for three times. The organic layers were combined and washed with water (10 mL) and brine (10 mL). The organic phase was dried over MgSO$_4$, filtered, concentrated, and purified by silica gel chromatography (EtOAc elution) to afford the acetylation compound. To a solution of the acetylation compound in MeOH (10 mL) was added K$_2$CO$_3$ (13 mg, 0.13 mmol). The mixture was stirred for 0.5 h at 26 °C, and then acidified to pH 5 by addition of Dowex 50WX8-200 cationic exchange resin. The resin was then removed by filtration. The filtrate was concentrated, and purified by silica gel chromatography (EtOAc, then MeOH/CH$_2$Cl$_2$ 1:4) to give pure compound **2** (146 mg, 27% yield).

5.2.2. Representative procedure B for Cu(I)-catalyzed (3 + 2) cycloaddition of alkyne and azide

The coupling reaction of 3,4-dihydroxycinnamic acid (540 mg, 3.0 mmol) with propargylamine (198 mg, 3.6 mmol) was performed in the presence of EDCI, HOBt and Et$_3$N in anhydrous DMF at 27 °C for 18 h to give the caffeic amide **17** (610 mg, 93% yield). A solution of 1,4-bis(azidomethyl)benzene [50] (**20**, 45.2 mg, 0.24 mmol), CuSO$_4$•5H$_2$O (5.2 mg, 0.024 mmol), sodium ascorbate (4.8 mg, 0.024 mmol) and caffeic amide **17** (126 mg, 0.58 mmol) in H$_2$O/THF (1:1, 10 mL) was stirred at 40 °C for 12 h, and then concentrated under reduced pressure. The residue was washed with water (2 × 10 mL), EtOAc (2 × 10 mL), and CH$_2$Cl$_2$ (2 × 10 mL),

and dried under reduced pressure to give compound **7** (102 mg, 67% yield).

5.3. Aβ preparation

For ThT assay, Aβ(1−42) peptides (Biopeptide, San Diego, CA) were dissolved in hexafluoroisopropanol (HFIP) in 1 mg/mL. The sample was mixed vigorously using a vortex for 5 s and then sonicated for 5 min. After 1 h, HFIP was evaporated in vacuum, and Aβ peptides were dissolved by anhydrous dimethylsulfoxide (DMSO) in 16 mg/mL, and diluted in 20 mM phosphate buffer (PB), pH 7.4. The final Aβ concentration was 50 μM and final DMSO concentration was 1.5%.

For ESI-TWIM-MS experiment, 0.12 mg Aβ(1−40) was first dissolved in 8 μL DMSO containing 10 mM diCA (**2**) and diluted into 800 μL, 50 mM ammonium acetate, at pH 6.8. The final DMSO concentration was 1%. Aβ(1−40) and diCA mixture was centrifuged at $11,000 \times g$ for 10 min before injection.

To prepare preformed Aβ(1−42) fibrils, 0.1 mg Aβ(1−42) was dissolved in 6 μL DMSO and diluted into 880 μL, 20 mM PB at pH 7.4. The solution was incubated in tubes for at least 4 days with continuous shaking.

5.4. ThT assay

Aβ(1−42) solution (50 μM) was prepared in PB (20 mM, pH = 7.4) with addition of 5 μM thioflavin T (ThT) in the absence or presence of test compound (0.01, 0.1, 0.8, 3.1, 12.5, 25 or 100 μM). The samples were incubated at 37 °C with agitation for 1 min every hour. ThT fluorescence was monitored using an ELISA microplate reader SpectraMax M5 (Molecular Devices, Sunnyvale, CA) with an excitation wavelength at 442 nm and emission at 485 nm. The ThT intensity was recorded at intervals over a period of 80 h incubation. Measurements from independent triplicate experiments were averaged and the standard error of mean (SEM) was calculated. To calculate IC$_{50}$, the final ThT intensity (at 80 h) of each condition (buffer background subtracted) was first normalized to Aβ(1−42) alone and the percentage of inhibition was calculated and averaged. The normalized final ThT intensity was plotted against compound concentration and the data were fitted to obtain half maximal inhibitory concentration (IC$_{50}$).

For disassembling experiments, the same volume of preformed Aβ(1−42) fibril solution was mixed with different concentrated compound **2**. ThT intensity was monitored as previously described.

5.5. Transmission electron microscopy

Aliquots (5 μL) of the end-point products from ThT assay (see section 5.4) were deposited onto 400-mesh Formvar carbon-coated copper grids (EMS electron Microscopy Sciences, Hatfield, PA, USA) for 5 min. The grids were blotted, washed once in droplets of Milli-Q water, and stained with 2% uranyl acetate. The samples were examined with a FEI Tecnai G2 TF20 Super TWIN transmission electron microscope with an accelerating voltage of 120 kV.

5.6. Gel electrophoresis and western blot

Twenty μL Aβ(1−42) fibrils incubated with or without diCA were diluted with 5 μL sodium dodecyl sulfate (SDS) sample buffer and loaded on the native 13% Tris-tricine gel without SDS. Separated Aβ(1−42) species on the gel were electrophoretically transferred to a nitrocellulose membrane at 250 mA for 75 min at 4 °C. The membrane was blocked with 5% skim milk. Proteins were detected by 4G8 and 6E10 antibodies and anti-mouse IgG secondary

antibody and visualized by enhanced chemiluminescence (ECL) detection kit.

5.7. LDH toxicity assay

The end products of ThT assay (see section 5.4) were subjected to SH-SY5Y cells, and the cytotoxicity was determined by LDH assay. CytoTox96 NonRadioactive Cytotoxicity Assay (Promega, Madison, WI) was performed according to the manufacturer's instruction. The human neuroblastoma SH-SY5Y cells (ATCC #CRL-2266) were incubated at 37 °C under 5% CO_2 and cultured in DMEM/F12 media with 5% fetal bovine serum (FBS). Cells were seeded in a 96-well microplate with 10,000 cells/well and incubated for 24 h. The media were discarded, and media without FBS were added. After adding 10 μL Aβ sample (i.e. the end product of ThT assay), the mixture was incubated for 24 h. Media were spun at $13,300 \times g$ for 5 min at 4 °C. Fifty μL medium was transferred and incubated with 50 μL reconstituted substrate for 30 min at room temperature in darkness. Reaction was stopped by adding 50 μL stop solution, then absorbance was read at 490 nm using a microplate reader SpectraMax M5 (Molecular Devices, Sunnyvale, CA). Background absorbance due to plain neuron medium without cells was subtracted from all readings. The signals were normalized to a positive control in which the cells were lysed by 2% Triton X-100 for 100% cytotoxicity.

5.8. Transgenic AD C. elegans paralysis analysis

Average number 130 eggs of *C. elegans* strains CL4176 *smg-1(cc546)*; *dvIs27[myo-3p::Aβ(1–42) + rol-6(su1006)]* were cultured on Nematode Growth Media (NGM) plates with *E. coli* strain OP5O at 16 °C and each plate was pretreated with 40 μL curcumin, CA, or diCA solution which were prepared at a concentration of 6.27 mM. Paralysis assays were initiated by raising the temperature to 25 °C when eggs larvae reached into L4 stage. The number of survival worms was counted every 2 h and five trials of each condition were repeated.

5.9. Electrospray ionization–traveling wave ion mobility–mass spectrometry (ESI-TWIM-MS)

The experiments were conducted on a Waters Synapt G2 HDMS instrument with a LockSpray ESI source, using the following parameters: ESI capillary voltage, 3.0 kV; sample cone voltage, 40 V; extraction cone voltage, 0 V; desolvation gas flow, 800 L/h (N_2); trap collision energy (CE), 4 V; transfer CE, 0 V; trap gas flow, 2.0 mL/min (Ar); source temperature, 100 °C; and desolvation temperature, 300 °C. Backing pressure was 2.28 mbar and time of flight (TOF) pressure was 2.3×10^{-7} mbar. The reference compound used for the lock-mass correction was leucine enkephalin ($[M + H]^+ = 556.2771$ Da). Samples were infused into the ESI source at a flow rate of 6 μL/min by a syringe pump (KDS-100, KD Scientific). For IMS experiments, the helium cell gas flow was held at 180.0 mL/min and the ion mobility cell gas flow was held at 90.0 mL/min (N_2). The DC traveling wave velocity and height were set as 683 m/s and 26.3 V, respectively. Data were collected and analyzed by using MassLynx 4.1 and DriftScope 2.4 (Waters). The CCS calibration curve was established according to the reported protocol [51,52], using published CCSs of cytochrome *c* (bovine), reserpine, lysozyme, insulin (human), and polyalanine [53–57]. A plot of corrected drift times *vs.* CCSs of calibrants fitted with power functions was used for experimental CCS measurements.

5.10. Docking studies and MD simulation

A partially folded structure of Aβ(1–40) in an aqueous environment (PDB coded 2LFM) was applied for molecular docking using Glide of Schrödinger Program Suite (Schrödinger Inc.). Initially, the diCA molecular structure was prepared and energy minimized by LigPrep and was docked flexibly to each of the 20 structural conformers of Aβ(1–40) by using Glide under extra-precision (XP) mode. Finally, from the structure clusters of all docked poses, eleven complexes of diCA with Aβ(1–40) were elected as the input structures for simulation works. MD simulation was performed by Desmond [58], implemented in the Schrödinger program suite (Schrödinger Inc.), with OPLS/AA force field. A simulation system was prepared by immersed diCA and Aβ complex into a cubic periodic box solvated by simple point charge water (SPC water). To neutralize the system, a minimum number of ions were added by randomly replace the system solvation molecules. After the system was built a steepest descent minimization with a maximum of 2000 steps was applied to minimize the system. A total 20 ns MD simulation was conducted with constant temperature (300 K) and pressure (1 bar) controlled by Nose-Hoover and Martyna-Tobias-Klein of molecule dynamics. A 9.0 Å cutoff for nonbond interaction was used. Electrostatic interaction was treated by Particle-mesh Ewald (PME). Energy and atomic coordinate trajectory was recorded every 1.2 and 4.8 ps. For each simulation, one hundred structures were extracted evenly through time, and each structure's CCS was calculated.

5.11. ^1H–^{15}N HSQC NMR

^{15}N-labeled Aβ(1–42) peptide was prepared via protein expression from BL21 Star (DE3) cells harboring pET14b-Aβ42 vectors [59]. Cells were transferred to M9 minimal medium before induction with 0.5 mM isopropyl β-ᴅ-1-thiogalactopyranoside (IPTG), and incubated for another 18–20 h at 37 °C. Protein purification was achieved following our previously developed method [59]. HSQC spectra of 25 μM of recombinant ^{15}N-labeled Aβ(1–42) peptide were acquired at 4 °C using Bruker Avance 600 MHz NMR spectrometer equipped with 5 mm triple resonance cryoprobe and Z-gradient. The concentration of diCA (**2**) is 0.5 mM. The peak assignment of $^{15}N/^1H$ chemical shifts referenced previous data deposited in the Biological Magnetic Resonance Data Bank (BRMB) and numbered 25218. Partially unsolved residues were assigned according to the spectra of Total Correlation Spectroscopy (TOCXY) performed on Bruker Avance 850 MHz NMR.

Author contributions

†L.-H.T., N.-H.T., and Y.-R.T. contributed equally to this work. L.-H.T., N.-H.T., Y.-R.T., T.-W.L., Y.-W.L, J.-L.C, Y.-S.C, and R.-J.C. conducted experiments. C.-S.C provided technical support and suggestion in worm studies. L.-H.T., N.-H.T., T.-W.L., Y.-D.W., and Y.-T.C. analyzed the data. L.-H.T., N.-H.T., J.-M.F., and Y.-R.C. wrote the manuscript. J.-M.F. and Y.-R.C. provided concepts and supervised the research.

Conflicts of interest

The authors have no conflicts of interest.

Appendix A. Supplementary data

Supplementary data related to this article can be found at https://doi.org/10.1016/j.ejmech.2018.08.084.

References

[1] D.J. Selkoe, Amyloid β-protein and the genetics of Alzheimer's disease, J. Biol. Chem. 271 (1996) 18295–18298.

[2] Y.L. Xiao, B.Y. Ma, D. McElheny, S. Parthasarathy, F. Long, M. Hoshi, R. Nussinov, Y. Ishii, Aβ(1-42) fibril structure illuminates self-recognition and replication of amyloid in Alzheimer's disease, Nat. Struct. Mol. Biol. 22 (2015) 499–505.

[3] M.A. Walti, F. Ravotti, H. Arai, C.G. Glabe, J.S. Wall, A. Bockmann, P. Guntert, B.H. Meier, R. Riek, Atomic-resolution structure of a disease-relevant Aβ(1-42) amyloid fibril, Proc. Natl. Acad. Sci. U.S.A. 113 (2016) E4976–E4984.

[4] R. Tycko, Molecular structure of amyloid fibrils: insights from solid-state NMR, Q. Rev. Biophys. 39 (2006) 1–55.

[5] L.C. Serpell, J.M. Smith, Direct visualisation of the β-sheet structure of synthetic Alzheimer's amyloid, J. Mol. Biol. 299 (2000) 225–231.

[6] M. Ewers, R.A. Sperling, W.E. Klunk, M.W. Weiner, H. Hampel, Neuroimaging markers for the prediction and early diagnosis of Alzheimer's disease dementia, Trends Neurosci. 34 (2011) 430–442.

[7] M. Wogulis, S. Wright, D. Cunningham, T. Chilcote, K. Powell, R.E. Rydel, Nucleation-dependent polymerization is an essential component of amyloid-mediated neuronal cell death, J. Neurosci. 25 (2005) 1071–1080.

[8] Y.R. Chen, C.G. Glabe, Distinct early folding and aggregation properties of Alzheimer amyloid-β peptides Aβ40 and Aβ42: stable trimer or tetramer formation by Aβ42, J. Biol. Chem. 281 (2006) 24414–24422.

[9] E.K. Esbjorner, F. Chan, E. Rees, M. Erdelyi, L.M. Luheshi, C.W. Bertoncini, C.F. Kaminski, C.M. Dobson, G.S.K. Schierle, Direct observations of amyloid β self-assembly in live cells provide insights into differences in the kinetics of Aβ(1-40) and Aβ(1-42) aggregation, Chem. Biol. 21 (2014) 732–742.

[10] L.D. Estrada, C. Soto, Disrupting β-amyloid aggregation for Alzheimer disease treatment, Curr. Top. Med. Chem. 7 (2007) 115–126.

[11] Q. Nie, X.G. Du, M.Y. Geng, Small molecule inhibitors of amyloid β peptide aggregation as a potential therapeutic strategy for Alzheimer's disease, Acta Pharmacol. Sin. 32 (2011) 545–551.

[12] T. Tomita, At the frontline of Alzheimer's disease treatment: γ-secretase inhibitor/modulator mechanism, N.-S. Arch. Pharmacol. 377 (2008) 295–300.

[13] X.-L. Bu, P.P.N. Rao, Y.-J. Wang, Anti-amyloid aggregation activity of natural compounds: implications for Alzheimer's drug discovery, Mol. Neurobiol. 53 (2016) 3565–3575.

[14] R.A. Cherny, C.S. Atwood, M.E. Xilinas, D.N. Gray, W.D. Jones, C.A. McLean, K.J. Barnham, I. Volitakis, F.W. Fraser, Y. Kim, X. Huang, L.E. Goldstein, R.D. Moir, J.T. Lim, K. Beyreuther, H. Zheng, R.E. Tanzi, C.L. Masters, A.I. Bush, Treatment with a copper-zinc chelator markedly and rapidly inhibits β-amyloid accumulation in Alzheimer's disease transgenic mice, Neuron 30 (2001) 665–676.

[15] A. Lorenzo, B.A. Yankner, β-amyloid neurotoxicity requires fibril formation and is inhibited by Congo red, Proc. Natl. Acad. Sci. U.S.A. 91 (1994) 12243–12247.

[16] W.E. Klunk, M.L. Debnath, J.W. Pettegrew, Chrysamine-G binding to Alzheimer and control brain: autopsy study of a new amyloid probe, Neurobiol. Aging 16 (1995) 541–548.

[17] F.S. Yang, G.P. Lim, A.N. Begum, O.J. Ubeda, M.R. Simmons, S.S. Ambegaokar, P.P. Chen, R. Kayed, C.G. Glabe, S.A. Frautschy, G.M. Cole, Curcumin inhibits formation of amyloid β oligomers and fibrils, binds plaques, and reduces amyloid in vivo, J. Biol. Chem. 280 (2005) 5892–5901.

[18] A.A. Reinke, J.E. Gestwicki, Structure-activity relationships of amyloid beta-aggregation inhibitors based on curcumin: influence of linker length and flexibility, Chem. Biol. Drug Des. 70 (2007) 206–215.

[19] V.S. Mithu, B. Sarkar, D. Bhowmik, A.K. Das, M. Chandrakesan, S. Maiti, P.K. Madhu, Curcumin alters the salt bridge-containing turn region in amyloid β(1-42) aggregates, J. Biol. Chem. 289 (2014) 11122–11131.

[20] K. Ono, K. Hasegawa, H. Naiki, M. Yamada, Curcumin has potent anti-amyloidogenic effects for Alzheimer's β-amyloid fibrils in vitro, J. Neurosci. Res. 75 (2004) 742–750.

[21] H. Endo, Y. Nikaido, M. Nakadate, S. Ise, H. Konno, Structure activity relationship study of curcumin analogues toward the amyloid-beta aggregation inhibitor, Bioorg. Med. Chem. Lett 24 (2014) 5621–5626.

[22] D. Yanagisawa, H. Taguchi, S. Morikawa, T. Kato, K. Hirao, N. Shirai, I. Tooyama, Novel curcumin derivatives as potent inhibitors of amyloid β aggregation, Biochem. Biophys. Rep. 4 (2015) 357–368.

[23] D. Sul, H.S. Kim, D. Lee, S.S. Joo, K.W. Hwang, S.Y. Park, Protective effect of caffeic acid against beta-amyloid-induced neurotoxicity by the inhibition of calcium influx and tau phosphorylation, Life Sci. 84 (2009) 257–262.

[24] M. Mammen, S.K. Choi, G.M. Whitesides, Polyvalent interactions in biological systems: implications for design and use of multivalent ligands and inhibitors, Angew. Chem. Int. Ed. 37 (1998) 2755–2794.

[25] C. Changtam, H.P. de Koning, H. Ibrahim, M.S. Sajid, M.K. Gould, A. Suksamrarn, Curcuminoid analogs with potent activity against trypanosoma and leishmania species, Eur. J. Med. Chem. 45 (2010) 941–956.

[26] H.C. Kolb, M.G. Finn, K.B. Sharpless, Click chemistry: diverse chemical function from a few good reactions, Angew. Chem. Int. Ed. 40 (2001) 2004–2021.

[27] K. Gade Malmos, L.M. Blancas-Mejia, B. Weber, J. Buchner, M. Ramirez-Alvarado, H. Naiki, D. Otzen, ThT 101: a primer on the use of thioflavin T to investigate amyloid formation, Amyloid 24 (2017) 1–16.

[28] X. Li, X. Zhang, A.R. Ladiwala, D. Du, J.K. Yadav, P.M. Tessier, P.E. Wright, J.W. Kelly, J.N. Buxbaum, Mechanisms of transthyretin inhibition of β-amyloid aggregation in vitro, J. Neurosci. 33 (2013) 19423–19433.

[29] J. Luo, S.K. Warmlander, A. Graslund, J.P. Abrahams, Non-chaperone proteins can inhibit aggregation and cytotoxicity of Alzheimer amyloid beta peptide, J. Biol. Chem. 289 (2014) 27766–27775.

[30] V. Domalain, V. Tognetti, M. Hubert-Roux, C.M. Lange, L. Joubert, J. Baudoux, J. Rouden, C. Afonso, Role of cationization and multimers formation for diastereomers differentiation by ion mobility-mass spectrometry, J. Am. Soc. Mass Spectrom. 24 (2013) 1437–1445.

[31] V. Domalain, M. Hubert-Roux, V. Tognetti, L. Joubert, C.M. Lange, J. Rouden, C. Afonso, Enantiomeric differentiation of aromatic amino acids using traveling wave ion mobility-mass spectrometry, Chem. Sci. 5 (2014) 3234–3239.

[32] K. Giles, S.D. Pringle, K.R. Worthington, D. Little, J.L. Wildgoose, R.H. Bateman, Applications of a travelling wave-based radio-frequency-only stacked ring ion guide, Rapid Commun. Mass Spectrom. 18 (2004) 2401–2414.

[33] S.D. Pringle, K. Giles, J.L. Wildgoose, J.P. Williams, S.E. Slade, K. Thalassinos, R.H. Bateman, M.T. Bowers, J.H. Scrivens, An investigation of the mobility separation of some peptide and protein ions using a new hybrid quadrupole/travelling wave IMS/oa-ToF instrument, Int. J. Mass Spectrom. 261 (2007) 1–12.

[34] L.M. Young, J.C. Saunders, R.A. Mahood, C.H. Revill, R.J. Foster, L.H. Tu, D.P. Raleigh, S.E. Radford, A.E. Ashcroft, Screening and classifying small-molecule inhibitors of amyloid formation using ion mobility spectrometry-mass spectrometry, Nat. Chem. 7 (2015) 73–81.

[35] A.A. Shvartsburg, R.R. Hudgins, P. Dugourd, M.F. Jarrold, Structural information from ion mobility measurements: applications to semiconductor clusters, Chem. Soc. Rev. 30 (2001) 26–35.

[36] S. Di Giovanni, S. Eleuteri, K.E. Paleologou, G.W. Yin, M. Zweckstetter, P.A. Carrupt, H.A. Lashuel, Entacapone and tolcapone, two catechol O-methyltransferase inhibitors, block fibril formation of α-synuclein and β-amyloid and protect against amyloid-induced toxicity, J. Biol. Chem. 285 (2010) 14941–14954.

[37] D. Giulian, L.J. Haverkamp, J.H. Yu, M. Karshin, D. Tom, J. Li, A. Kazanskaia, J. Kirkpatrick, A.E. Roher, The HHQK domain of β-amyloid provides a structural basis for the immunopathology of Alzheimer's disease, J. Biol. Chem. 273 (1998) 29719–29726.

[38] D. Giulian, L.J. Haverkamp, J.H. Yu, W. Karshin, D. Tom, J. Li, J. Kirkpatrick, L.M. Kuo, A.E. Roher, Specific domains of β-amyloid from Alzheimer plaque elicit neuron killing in human microglia, J. Neurosci. 16 (1996) 6021–6037.

[39] M.P. Williamson, Y. Suzuki, N.T. Bourne, T. Asakura, Binding of amyloid β-peptide to ganglioside micelles is dependent on histidine-13, Biochem. J. 397 (2006) 483–490.

[40] J. McLaurin, P.E. Fraser, Effect of amino-acid substitutions on Alzheimer's amyloid-β peptide-glycosaminoglycan interactions, Eur. J. Biochem. 267 (2006) 6353–6361.

[41] L.O. Tjernberg, J. Naslund, F. Lindqvist, J. Johansson, A.R. Karlstrom, J. Thyberg, L. Terenius, C. Nordstedt, Arrest of β-amyloid fibril formation by a penta-peptide ligand, J. Biol. Chem. 271 (1996) 8545–8548.

[42] M.M. Pallitto, J. Ghanta, P. Heinzelman, L.L. Kiessling, R.M. Murphy, Recognition sequence design for peptidyl modulators of β-amyloid aggregation and toxicity, Biochemistry 38 (1998) 3570–3578.

[43] S. Sambashivan, M.R. Sawaya, D. Eisenberg, 2ONV: crystal Structure of the Amyloid-fibril Forming Peptide GGVVIA Derived from the Alzheimer's Amyloid Aβ (Aβ37-42) in Worldwide Protein Data Bank, 2007.

[44] S. Vivekanandan, J.R. Brender, S.Y. Lee, A. Ramamoorthy, A partially folded structure of amyloid-beta(1-40) in an aqueous environment, Biochem. Biophys. Res. Commun. 41 (1) (2011) 312–316.

[45] M. Sunde, L.C. Serpell, M. Bartlam, P.E. Fraser, M.B. Pepys, C.C.F. Blake, Common core structure of amyloid fibrils by synchrotron X-ray diffraction, J. Mol. Biol. 273 (1997) 729–739.

[46] A.T. Petkova, Y. Ishii, J.J. Balbach, O.N. Antzutkin, R.D. Leapman, F. Delaglio, R. Tycko, A structural model for Alzheimer's β-amyloid fibrils based on experimental constraints from solid state NMR, Proc. Natl. Acad. Sci. U.S.A. 99 (2002) 16742–16747.

[47] T.H. Keller, A. Pichota, Z. Yin, A practical view of 'druggability', Curr. Opin. Chem. Biol. 10 (2006) 357–361.

[48] S.A. Hudson, H. Ecroyd, T.W. Kee, J.A. Carver, The thioflavin T fluorescence assay for amyloid fibril detection can be biased by the presence of exogenous compounds, FEBS J. 276 (2009) 5960–5972.

[49] T. Hill, L.R. Odell, J.K. Edwards, M.E. Graham, A.B. McGeachie, J. Rusak, A. Quan, R. Abagyan, J.L. Scott, P.J. Robinson, A. McCluskey, Small molecule inhibitors of

dynamin I GTPase activity: development of dimeric tyrphostins, J. Med. Chem. 48 (2005) 7781–7788.

[50] J.R. Thomas, X.J. Liu, P.J. Hergenrother, Size-specific ligands for RNA hairpin loops, J. Am. Chem. Soc. 127 (2005) 12434–12435.

[51] B.T. Ruotolo, J.L.P. Benesch, A.M. Sandercock, S.J. Hyung, C.V. Robinson, Ion mobility-mass spectrometry analysis of large protein complexes, Nat. Protoc. 3 (2008) 1139–1152.

[52] K. Thalassinos, M. Grabenauer, S.E. Slade, G.R. Hilton, M.T. Bowers, J.H. Scrivens, Characterization of phosphorylated peptides using traveling wave-based and drift cell ion mobility mass spectrometry, Anal. Chem. 81 (2009) 248–254.

[53] I. Campuzano, M.F. Bush, C.V. Robinson, C. Beaumont, K. Richardson, H. Kim, H.I. Kim, Structural characterization of drug-like compounds by ion mobility mass spectrometry: comparison of theoretical and experimentally derived nitrogen collision cross sections, Anal. Chem. 84 (2012) 1026–1033.

[54] M.F. Bush, I.D.G. Campuzano, C.V. Robinson, Ion mobility mass spectrometry of peptide ions: effects of drift gas and calibration strategies, Anal. Chem. 84 (2012) 7124–7130.

[55] K.B. Shelimov, D.E. Clemmer, R.R. Hudgins, M.F. Jarrold, Protein structure in vacuo: gas-phase conformations of BPTI and cytochrome c, J. Am. Chem. Soc. 119 (1997) 2240–2248.

[56] S.J. Valentine, J.G. Anderson, A.D. Ellington, D.E. Clemmer, Disulfide-intact and -reduced lysozyme in the gas phase: conformations and pathways of folding and unfolding, J. Phys. Chem. B 101 (1997) 3891–3900.

[57] R. Salbo, M.F. Bush, H. Naver, I. Campuzano, C.V. Robinson, I. Pettersson, T.J.D. Jorgensen, K.F. Haselmann, Traveling-wave ion mobility mass spectrometry of protein complexes: accurate calibrated collision cross-sections of human insulin oligomers, Rapid Commun. Mass Spectrom. 26 (2012) 1181–1193.

[58] K.J. Bowers, E. Chow, H. Xu, R.O. Dror, M.P. Eastwood, B.A. Gregersen, J.L. Klepeis, I. Kolossváry, M.A. Moraes, F.D. Sacerdoti, J.K. Salmon, Y. Shan, D.E. Shaw, Scalable algorithms for molecular dynamics simulations on commodity clusters, Proc. ACM/IEEE Conf. Supercomputing. SC'06 (2006) 1188544.

[59] Y.H. Liao, Y.R. Chen, A novel method for expression and purification of authentic amyloid-beta with and without ^{15}N labels, Protein Expr. Purif. 113 (2015) 63–71.